Geological Quarterly, 2019, **63** (3): 558–567
DOI: http://dx.doi.org/10.7306/gq.1485

Ideal body analysis of the Pomerania Gravity Low (northern Poland)

Zdzisław PETECKI[1, *]

[1] Polish Geological Institute – National Research Institute, Rakowiecka 4, 00-975 Warszawa, Poland

Petecki, Z., 2019. Ideal body analysis of the Pomerania Gravity Low (northern Poland). Geological Quarterly, **63** (3): 558–567, doi: 10.7306/gq.1485

Associate editor: Tomisław Gołębiowski

The large negative residual Bouguer gravity anomaly in northern Poland called the Pomerania Gravity Low (PGL) was analysed using Parker's ideal body theory. A residual gravity anomaly along the profile was inverted to find bounds on the density contrast, depth, and minimum thickness of its sources. As the ideal body reaches the surface, the greatest maximum negative density contrast is –0.038 g/cm^3, while the body itself has a thickness of 52 km. If 8 km is taken as a depth to the source body top, the density contrast must correspond to at least –0.092 g/cm^3, with a maximum allowable thickness of 18 km. The ideal body inversions show that the depth to the body top cannot exceed 15 km. Assuming a geologically reasonable maximum density contrast as small as –0.2 g/cm^3, the source body top can be no deeper than 11.5 km, and its thickness greater than or equal to 6 km, assuming it extends up to the Earth surface, or greater than or equal to 7 km, when its top is below 8 km depth. It can be hypothesized that the main source of the negative gravity anomaly is related to a predominance of felsic rocks in the Paleoproterozoic Dobrzyń Domain of the East European Platform basement.

Key words: gravimetry, Pomerania Gravity Low, ideal body analysis, northern Poland.

INTRODUCTION AND GEOPHYSICAL REGIONAL BACKGROUND

The Pomerania Gravity Low (PGL) in northern Poland, also known as the Lower Vistula River depression, is one of the most pronounced negative gravity anomalies in Poland with a minimum value of about –62 mGal (Królikowski and Petecki, 1995). This northwest-trending anomaly, elliptical in shape, has the longer dimension of about 250 km and is about 150 km across. It extends parallel and close to the Teisseyre-Tornquist Zone (TTZ) – a major discontinuity separating the thick and cold lithosphere of the Precambrian East European Platform from the much thinner and hotter Paleozoic Platform extending to the SW (Fig. 1; see the recent regional review in Narkiewicz et al., 2015). Geological map of crystalline basement in the Polish part of the East European Platform (Krzemińska et al., 2017) shows the Paleoproterozoic granitic Dobrzyń Domain in the area of the PGL (Fig. 1).

The crust and uppermost mantle architecture in that area has been imaged by wide-angle reflection and refraction (WARR) seismic profiles (Guterch and Grad, 2006). The seismic velocity (V_p) models present the three-layered crystalline crust of the East European Platform (Fig. 2). The major features of the crust structure are the inclined top of the crystalline basement and an associated regional thickening of Paleozoic-Mesozoic sediments toward the platform boundary, as well as corresponding inclinations of intracrustal boundaries and the Moho toward the TTZ.

The PGL anomaly was interpreted to be caused by a crustal source, with its top located no deeper than 10 km below the surface, and the thickness greater than or equal to 2.7 km (Młynarski et al., 1982). According to the gravity data analyses, this anomaly may be caused by lower densities of rocks in the upper crystalline crust (Grabowska and Raczyńska, 1991; Grabowska et al., 1992). Fajklewicz (1964) suggested that the anomaly is connected with the Moho topography in this area. Other authors argued that the PGL is due to the superimposed gravity effects of the Moho topography and the lower-density upper part of the sedimentary cover (Grabowska et al., 1998).

Królikowski and Petecki (1995) and Królikowski et al. (1998) suggested that this anomaly has been influenced by less dense rocks of the crystalline basement. The above authors argued that the connection of the anomaly with the sedimentary cover is contradicted by the following evidence: (1) results of removal of the gravity effect of the Permian-Cenozoic cover from the Bouguer gravity anomalies (Grobelny and Królikowski, 1988); (2) presence of the Lower Paleozoic rocks in the deep sedimentary cover, consisting mostly of Silurian rocks of almost constant, relatively high density (2.65 g/cm^3); and (3) smooth morphology of the top of the Precambrian crystalline basement evidenced by the seismic refraction data (Fig. 2). Some gravity models along profiles crossing the Trans-European Suture Zone in north-west Poland (Królikowski and Petecki, 1997,

* E-mail: zdzislaw.petecki@pgi.gov.pl

Received: February 28, 2019; accepted: June 14, 2019; first published online: September 3, 2019

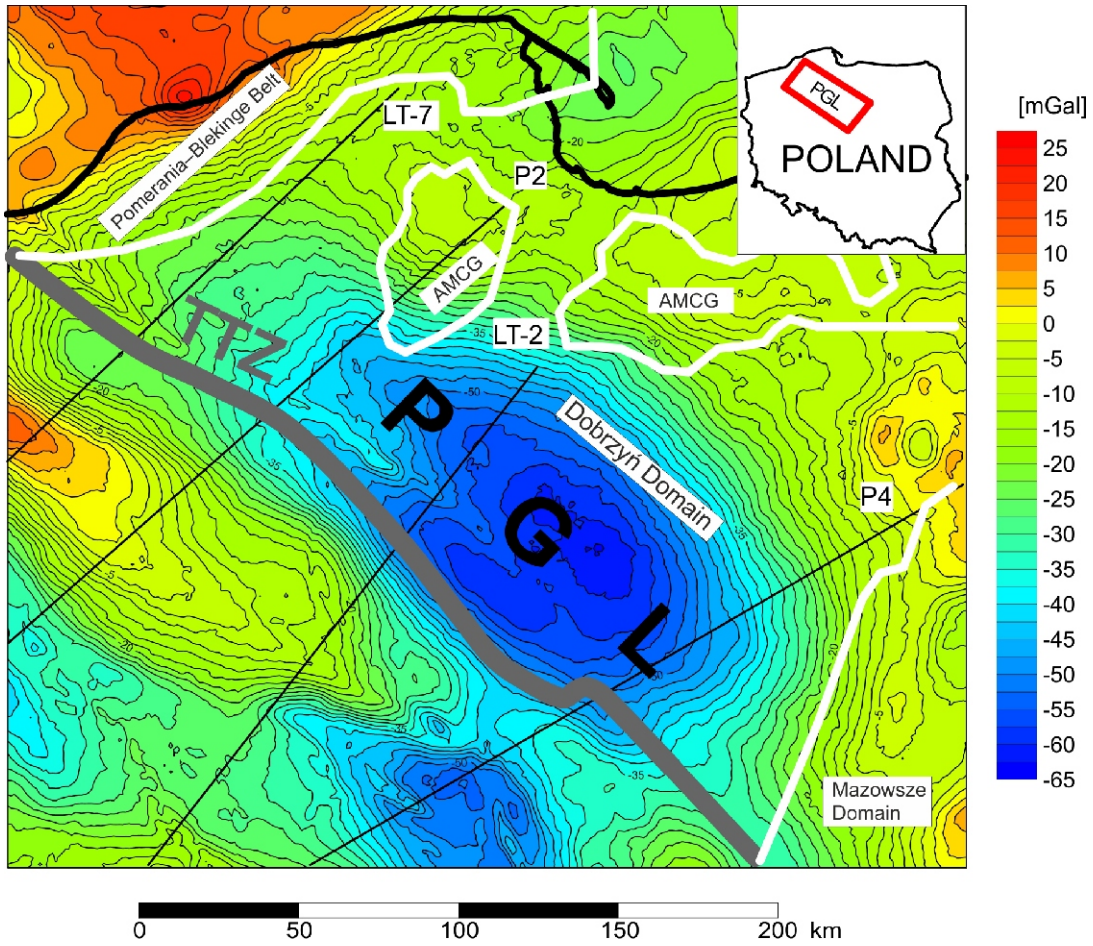

Fig. 1. Bouguer gravity anomaly map of the research area, and the sketch of main geological domains of the EEC (boundaries marked by white lines) after Krzemińska et al. (2017)

AMCG – anorthosite–mangerite–charnockite–granite suite rock; PGL – Pomeranian Gravity Low; TTZ – Teisseyre-Tornquist Zone after Narkiewicz et al. (2015); LT-7, P2, LT-2, P4 – WAAR seismic profiles

2002; Petecki, 2002, 2008), which are primarily based on the velocity models along WARR seismic profiles, demonstrate a low-density uppermost mantle and a crust thickening in the area of the PGL.

The recent gravity models (Mazur et al., 2015, 2016a, b) show a narrow crustal keel as an important contribution to the PGL. The cited authors proposed that the modelled keel is in fact a trace of the TTZ actually representing a Precambrian intracratonic suture. Narkiewicz and Petecki (2016, 2017) argued against this new concept of the TTZ, stressing, among other arguments, that the crustal keel model is not well constrained by gravity and seismic data.

The above short review of the different interpretations of the PGL demonstrates that the origin of this anomaly is a subject of various hypotheses and is still far from final solution. In this context, it is worth noting that density interpretation of gravity anomalies is mathematically non-unique and different geological models can fit the observed data (Blakely, 1995). The gravity models of the PGL have a strong bearing on contrasting interpretations of the geological structure of northern Poland. Therefore, the aim of this paper is to use a classical approach to the gravity interpretation, which is not restricted to the specific source geometries. Thus, the theory of ideal bodies (Parker, 1974, 1975) has been applied to a gravity profile crossing the PGL anomaly to find bounds on the density contrast, maximum depth and minimum thickness of the anomalous body, using the algorithm presented by Huestis and Ander (1983).

MATERIALS AND METHODS

GRAVITY DATA

The simple Bouguer gravity anomaly map (Fig. 1) has been prepared using gravity measurements with a sampling density of about 1.6 stations/km^2. The gravity data were tied to the gravity datum based on the IGSN 71 (International Gravity Standarization Net of 1971). The Bouguer anomalies have been calculated using a reduction density of 2250 kg/m^3 (2.25 g/cm^3), corresponding to a mean density of rocks occurring in the Polish Lowland above sea level, and the GRS 80 (Geodetic Reference System of 1980) formula for the theoretical gravity (Królikowski and Petecki, 1995).

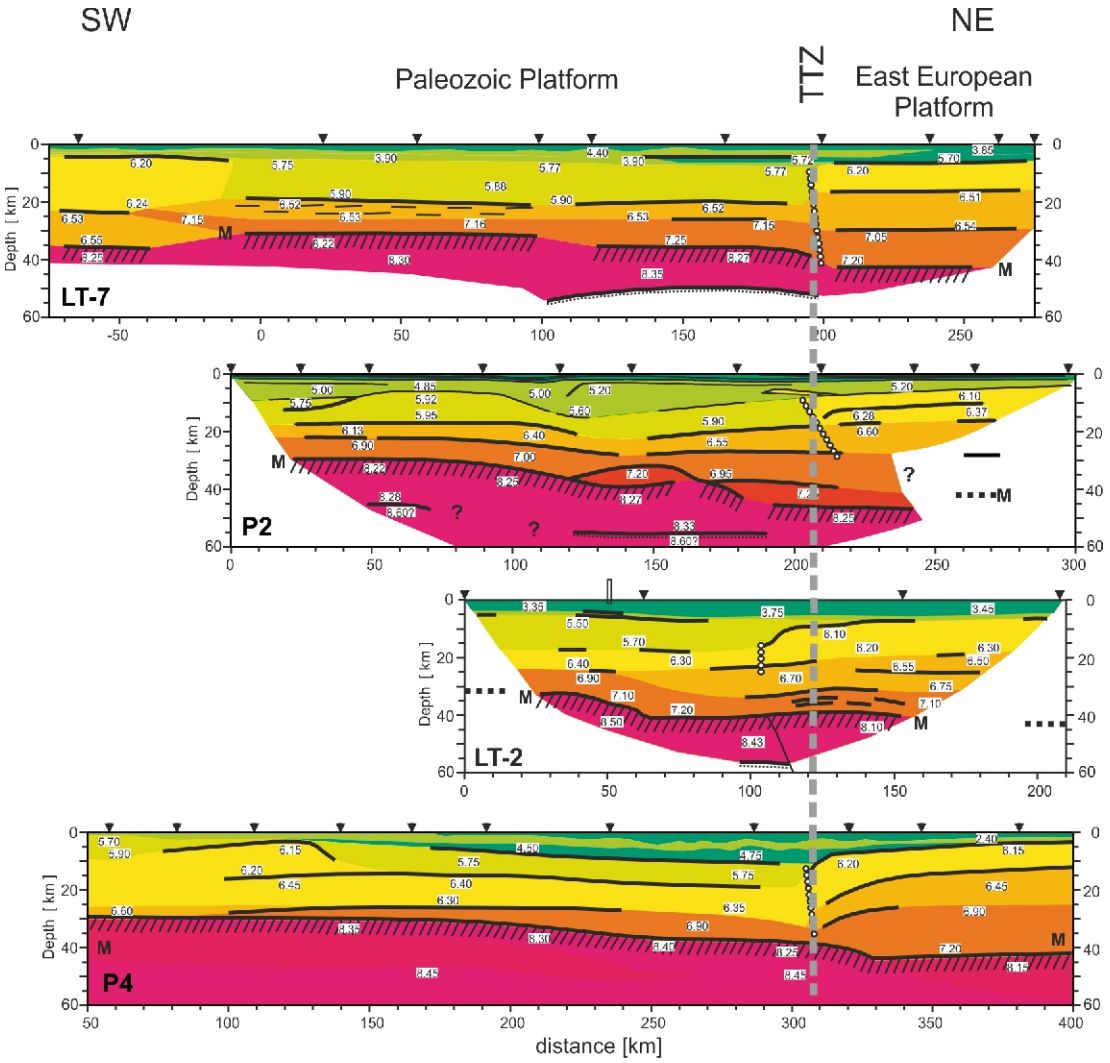

Fig. 2. P-wave velocity structure for LT-7, P2, LT-2 and P4 profiles (after Guterch and Grad, 2006)

Numbers in white boxes are velocities in km/s

In order to reproduce best the long wavelength nature of the PGL, a low-pass filtered gravity anomaly with a cut-off wavelength of 50 km was chosen for the gravity interpretation. This cut-off wavelength suppresses short-wavelength features that are not a subject of the present study, as the main focus is given to the large-scale regional structure responsible for the PGL. The resulting gravity anomaly is shown in Figure 3, as well as the location of the A–A' profile discussed in this paper.

The gravity data along the SW–NE-trending A–A' gravity profile crossing the PGL and perpendicular to the major axis of the anomaly were extracted from the low-pass filtered (smoothed) Bouguer anomaly map (Fig. 3). The gravity profile A–A' is illustrated in Figure 4A.

One of the most important problems in the interpretation of gravity measurements is that of separating the gravity field into its regional and residual components. In the case under study, the primary interest was in obtaining a residual gravity anomaly which would help in defining the bounds on density contrast, depth, and minimum thickness of its source. The task is by no means trivial due to the broadband nature of the analysed anomaly.

Consistent with this purpose it was assumed that the best estimate of the background regional gravity field for the low-pass filtered PGL anomaly is –5.77 mGal; the value of the field at the NE end of profile A–A'. It was also assumed that the regional field has a linear trend inclined to the SE (Fig. 4A). This regional trend of 0.12 mGal/km was subtracted from the smoothed PGL anomaly to obtain the residual anomaly with a minimum value of about –47 mGal.

The residual gravity anomaly along the A–A' profile is analyzed below using Parker's ideal-body theory to obtain bounds on the density contrast, depth, and minimum thickness of the causative body.

GRAVITY IDEAL BODY

Interpretation of gravity anomalies usually involves construction of a density model that satisfies the observed data. Unfortunately, this process is mathematically non-unique since gravity data are compatible with an infinite number of density solutions (e.g., Blakely, 1995). Parker (1974, 1975) proposed a more general approach to the gravity interpretation, which is based on finding certain fundamental properties that are common to the entire infinite set of density models and that are not restricted to specific source geometries. Parker's theory characterizes the extreme solution with the smallest possible maxi-

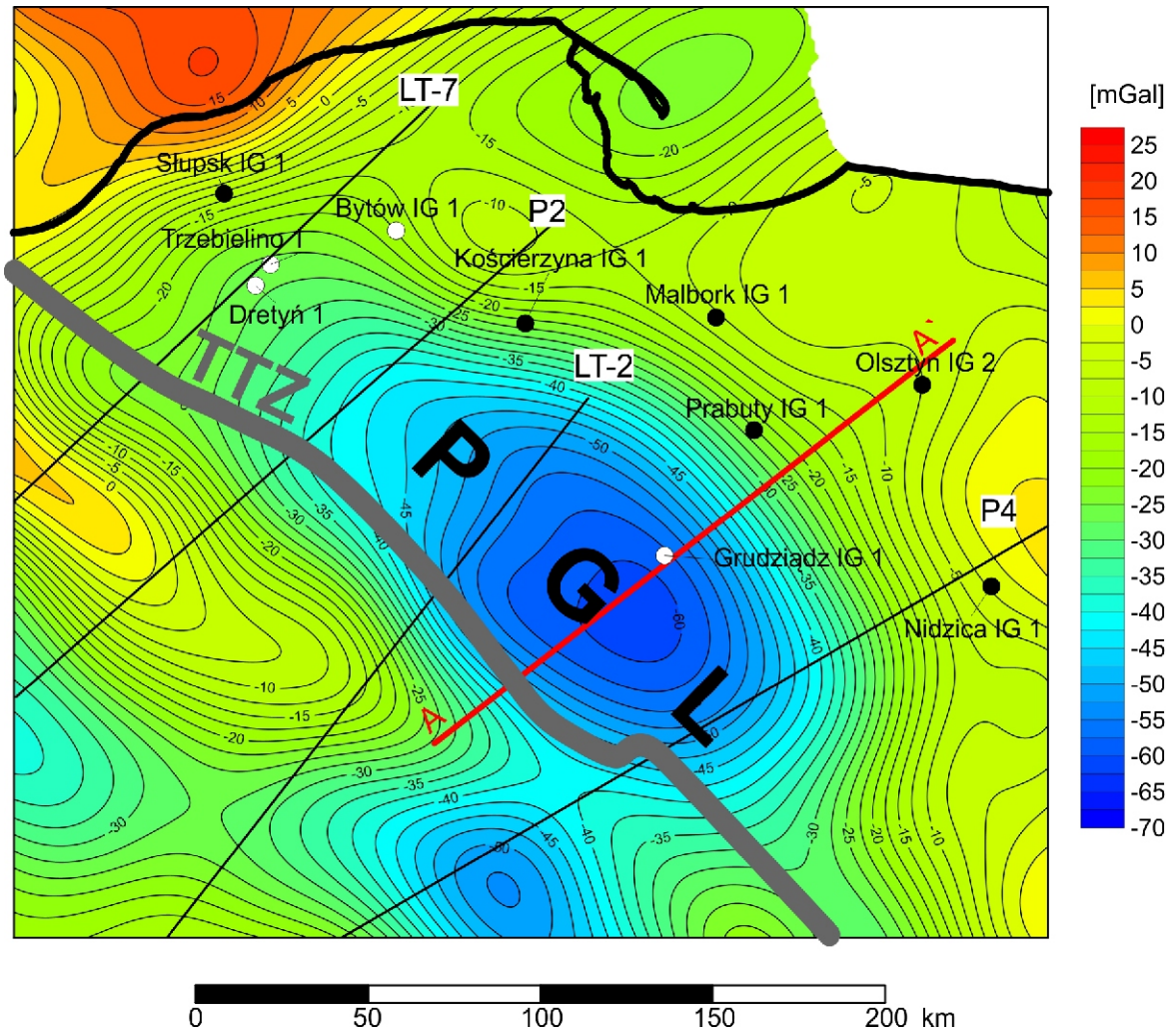

Fig. 3 Low-pass filtered gravity anomaly map

PGL – Pomeranian Gravity Low; TTZ – Teisseyre-Tornquist Zone; LT-7, P2, LT-2, P4 – WAAR seismic profiles; Bytów IG 1, Dretyń 1, Trzebielino 1, Grudziądz IG 1 – boreholes that drilled Silurian rocks; Kościerzyna IG 1, Malbork IG 1, Nidzica IG 1, Olsztyn IG 2, Prabuty IG 1 – boreholes piercing the crystalline basement top; A–A' – gravity profile used for ideal body inversion

mum density contrast that can explain the anomaly within a given misfit. The corresponding unique solution, the so-called ideal body, means that any source located at a particular depth must somewhere have a density contrast at least as great as the density contrast of the ideal body. In other words, there are infinitely more sources of higher density that will explain the anomaly, and none of lower density.

However, Parker's analytical method is suitable only for two measured data and a homogeneous ideal body with positive density contrast $_0$ (Parker, 1974). When more than two data are used, the ideal body analytical solution can be approximated by an extreme solution which has the smallest possible maximum positive density contrast $_0$ satisfying the observed anomaly for given data and their misfits s_i in a specified region of solution confinement (Parker, 1975; Huestis and Ander, 1983; Huestis, 1986; Ander and Huestis, 1987).

The algorithms, which are based on linear programming techniques, may be used to estimate the extreme solutions. In such an approach, it is assumed that the observed gravimetric anomaly is described by a discrete set of data (g_i, i = 1, 2, …, n) with associated maximum allowable misfits $_i$, and the region of source confinement is divided into m cells, with $m >> n$, each of own constant density $_j$. It is also assumed that all acceptable solutions are nonnegative ($_j$ 0).

The objective in that case is to minimize upper limitation $_0$ for all $_j$ parameters such that $_j$ $_0$ for all j = 1, 2,..., m subjected also to the following constraints (Huestis and Ander, 1983):

$$g_i \quad \sum_{j\ 1}^{m} a_{ij}\ _j \quad e_i \qquad i = 1, 2, ...n$$

$$_i \quad e_i \quad _i \qquad i = 1, 2, ...n$$

and

$$_j \quad 0 \qquad j = 1, 2, ...m$$

where: $_j$ – the density of the jth domain, e_i – the assumed acceptable misfit for the ith measuring point, and a_{ij} – the model gravity anomaly at data location i corresponding to the jth source domain with unit density attributed to it.

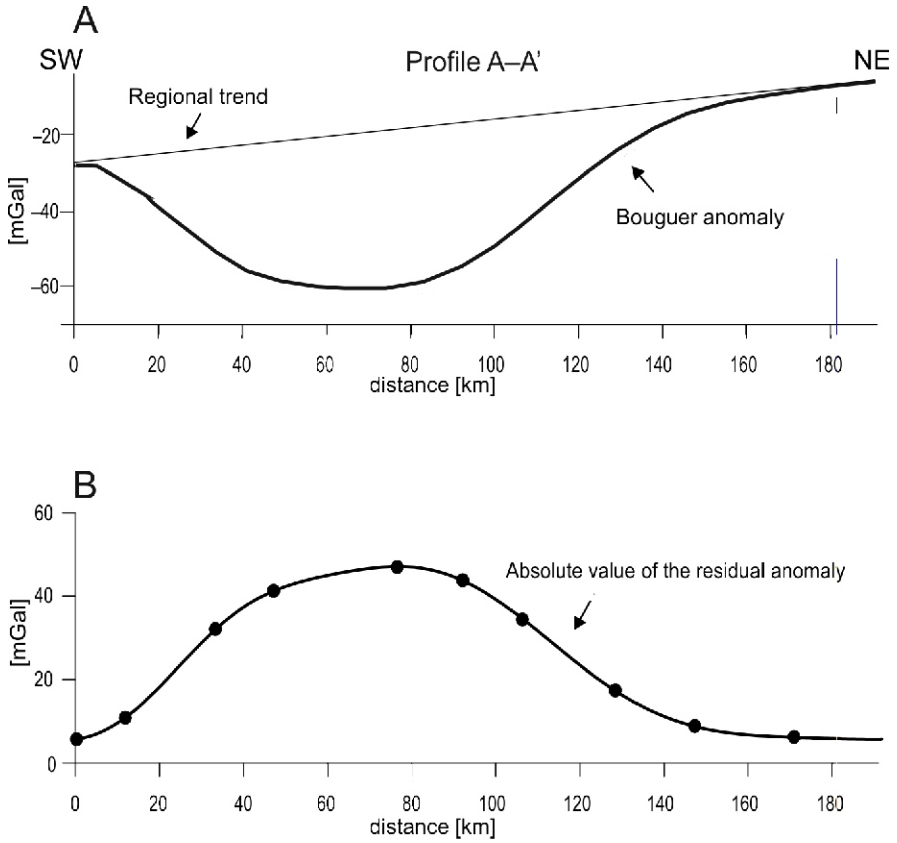

Fig. 4A – gravity profile A–A' (see Fig. 3 for location) used to calculate ideal body parameters, and the subtracted linear regional trend; B – residual gravity anomaly and gravity data points used in the ideal body analysis

This procedure is the so-called ideal body inversion.

The density contrast $_0$ depends not only on the data values and assumed allowed levels of their misfits but also on the region of equivalent sources confinement. Thus, the limits of this region can be varied to study the corresponding variation in the density bound. It must be stressed that an ideal body always touch the top of the region of sources confinement (Ander and Huestis, 1987).

The set of solutions of the ideal body inversion are presented in terms of trade-off diagrams, where the smallest possible limitation $_0$ for the density contrast is plotted as a function of the assumed maximal depth to the top (or assumed minimal thickness, when the top is fixed) of the causative body (Huestis and Ander, 1983). These trade-off curves define the regions of possible density solutions consistent with the observations which are located on the convex side of these trade-off curves.

Moreover, if the maximum density contrast of the source (a geological bound) can be assumed, the maximal possible source top depth or minimal thickness of the source (when the top depth is fixed) can be estimated (Blakely, 1995). For example, when at some depth to top, the density contrast of ideal body starts to exceed the maximal allowed density contrast, this depth is then the maximal possible depth to the source. On the other hand, if the depth to source can be constrained by, e.g., the well data, then bounds on the density contrasts can be obtained.

The ideal body theory was applied to interpret the origin of the PGL anomaly. Bounds on the density contrast have been computed using the absolute data values of residual anomaly along profile A–A' (Fig. 4B) to satisfy the non-negative condition required by the inversion algorithm (Huestis and Ander, 1983). Ten data points sampled from the residual gravity profile have been inverted to find the subsurface structures with the smallest possible maximum density contrast required to explain the anomaly. A misfit of 0.25 mGal was assumed for the gravity values used in the calculations. The Fortran program of Huestis and Ander (1983), modified by the present author to be capable of treating the 2.5 D interpretation approach and up to 1000 cells, has been used to calculate ideal bodies.

The region of confinement was partitioned into rectangular cells whose horizontal and vertical dimensions along the profile were 5 and 2 km, respectively, while their lateral extent was ±50 km in the direction perpendicular to the profile. The cell size has been kept constant for the calculations, while the number of cells and the dimensions of the region of confinement have been chosen properly in each of the presented optimization tasks.

RESULTS

A series of optimizations were performed modifying either the depth to the top or the thickness of the causative body to find the subsurface structure of the PGL source with the smallest possible maximum density contrast confined to a particular region (Figs. 5–8). Taking into account that the residual PGL anomaly has negative values, and therefore the actual density solution values must be negative, the opposite sign of computed density contrast is used further in the text.

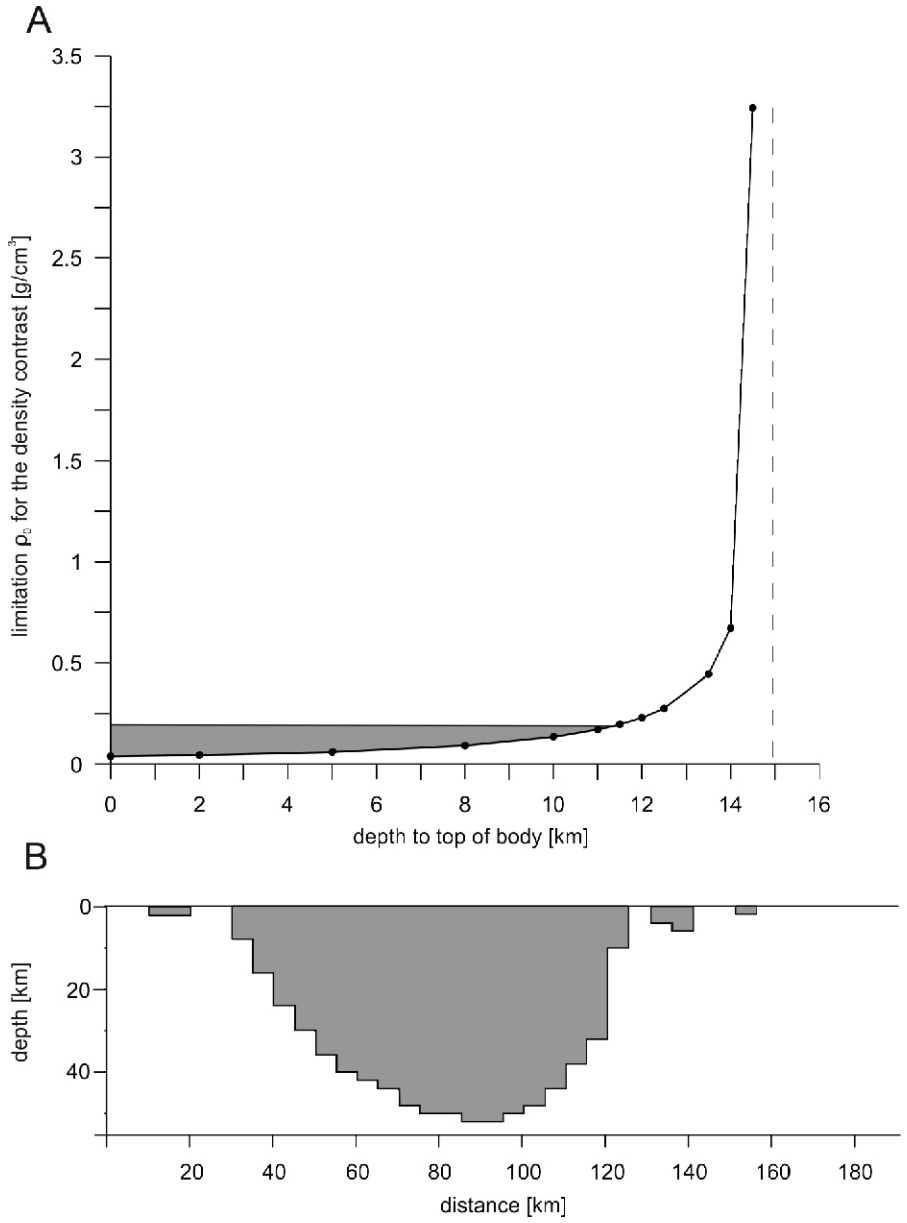

Fig. 5A – the smallest possible limitation $_0$ for the density contrast depicted as a function of the assumed depth to top of an ideal body having its bottom not limited by depth constraint (solid line and dots); the solution is possible if the ideal body top is shallower than 15 km; the maximum depth is 11.5 km assuming a maximum density contrast of 0.2 g/cm^3; shaded area indicates the region of feasible solutions; B – ideal body density cross-section for the solution computed assuming that its upper boundary is located at the surface, while the bottom depth is not fixed

DEPTH TO THE TOP OF IDEAL BODY

The ideal body for gravity profile A–A' was first computed assuming that its upper boundary is located at the surface, while the bottom depth is not fixed. The result points to the greatest possible negative density contrast of –0.038 g cm^{-3} (Fig. 5A), with a maximum allowable thickness of 52 km (Fig. 5B) for the source body. In accordance with the ideal body theory, such a result indicates that the PGL anomaly data and their misfits cannot be fit by any structure with larger negative density contrasts, i.e. greater than –0.038 g cm^{-3}.

In a subsequent series of calculations, the depth to the top of the body was increased to find the greatest negative density contrast for various body depths. The values of density contrasts obtained are shown in Figure 5A as a function of the depth to the top of the region of confinement of the solution source body. This trade-off curve gives the bound on the infinite number of density solutions which are located on the convex side of this trade-off curve. For example, if the source of the PGL is confined below 2.7 km depth, the density contrast cannot be everywhere greater than –0.043 g/cm^3, but if it is confined below 8 km depth the density contrast cannot be everywhere greater than –0.092 g/cm^3. There is no solution if the ideal body top is deeper than 15 km.

If the density contrast is assumed to be –0.2 g/cm^3, then the maximum depth to the body top is about 11.5 km.

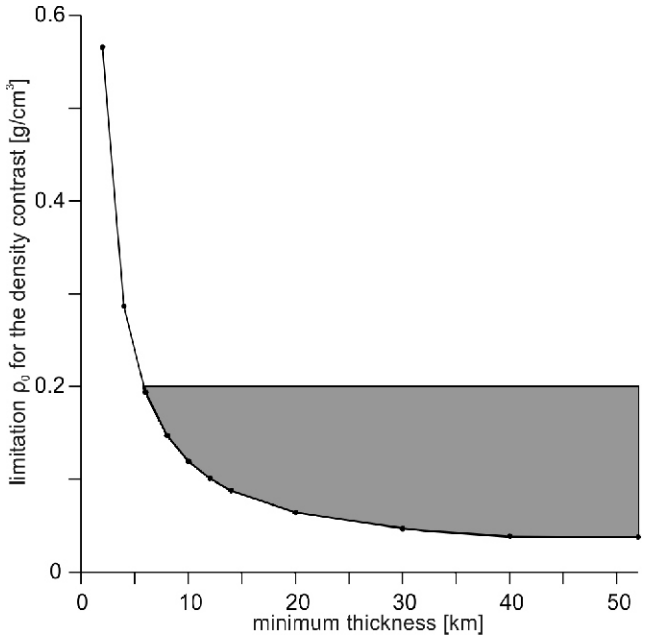

Fig. 6. The smallest possible limitation $_0$ for the density contrast of the ideal body having its top at the surface, depicted as a function of the body allowable thickness (solid line and dots)

The minimum thickness is 6 km, assuming a maximum density contrast of 0.2 g/cm^3; shaded area indicates the region of feasible solutions

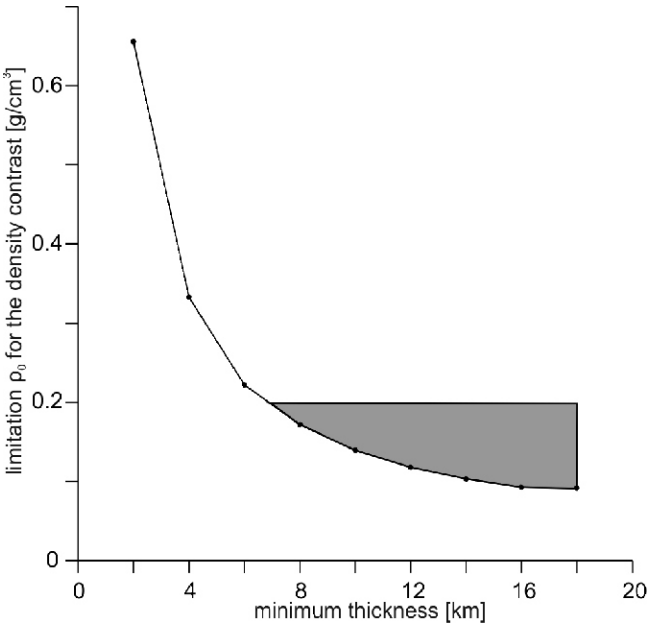

Fig. 8. The smallest possible limitation $_0$ for the density contrast of the ideal body having its top below 8 km depth, depicted as a function of the body allowable thickness (solid line and dots)

The minimum thickness is 7 km, assuming a maximum density contrast of 0.2 g/cm^3; shaded area indicates the region of feasible solutions

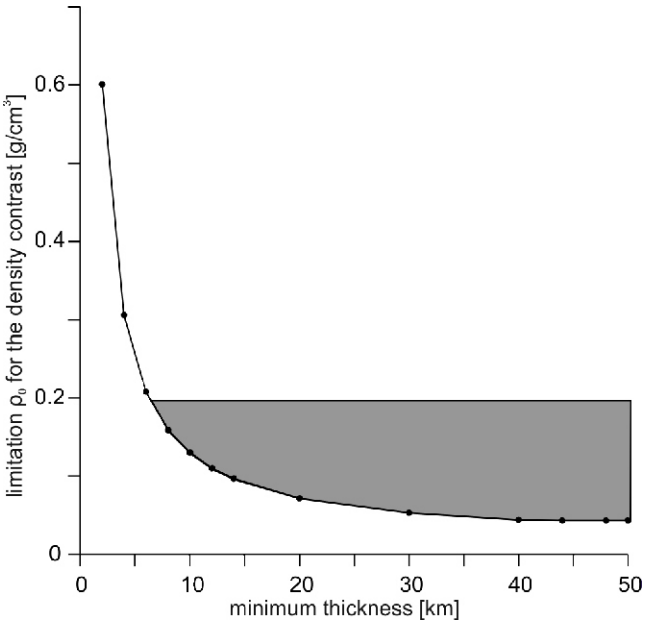

Fig. 7. The smallest possible limitation $_0$ for the density contrast of the ideal body having its top below 2.7 km depth, depicted as a function of the body allowable thickness (solid line and dots)

The minimum thickness is 6.35 km, assuming a maximum density contrast of 0.2 g/cm^3; shaded area indicates the region of feasible solutions

THICKNESS OF THE IDEAL BODY

In the next step of interpretation, the body top has been fixed at the surface or at a specified depth, and the depth to the bottom has been modified. From these calculations, the smallest maximum density contrasts as a function of depth to the bottom or thickness of the body have been obtained. For this case, the values of density contrasts are plotted for corresponding values of thickness or depth to the bottom on the trade-off curve providing bounds on the infinite set of density solutions located in the convex region of the graph. This curve can be used in a fashion similar to that given above (Fig. 5) to determine the minimum thickness of the source.

Figure 6 shows the smallest maximum density contrast for various ideal bodies which have their tops at the surface and which have variable thicknesses. The curve in this figure indicates the greatest maximum density contrast of –0.038 g/cm^3 (see also Fig. 5), with a maximum allowable thickness of 52 km for the source body. The minimum thickness of the ideal body is 6 km for the above assumed density contrast –0.2 g/cm^3.

Next, it is assumed that the average depth to the Lower Paleozoic strata (2.7 km) is taken as the upper limit on the depth to the top of the ideal body. Figure 7 shows the smallest maximum density contrast for various ideal bodies confined below 2.7 km depth, and which have variable thicknesses. The curve indicates the greatest maximum density contrast of –0.043 g/cm^3, with a maximum allowable thickness of 50 km for the source body. The minimum thickness is 6.35 km, assuming a density contrast of –0.2 g/cm^3.

It is further assumed that the maximum depth to crystalline basement, i.e. 8 km (Fig. 2), is taken as the limit on the depth to the top of the ideal body. Under such assumption, the greatest maximum density contrast is –0.092 g/cm^3, with a maximum allowable thickness of 18 km for the source body (Fig. 8). Assuming the density contrast of –0.2 g/cm^3, the source body can be no thinner than 7 km. Thus, confining the body below 2.7 km or 8 km does not substantially increase the minimum thickness of the anomalous body.

DISCUSSION

Analysis of the gravity data for the A–A' profile using the ideal body theory defines the allowed ranges of parameters of feasible solutions for the source of the PGL. All solutions lying within convex zones of the trade-off curves shown in Figures 5–8 are consistent with the constraints imposed in the inversion procedure. Accordingly, taking into account that the real density solution values must be negative, the greatest density contrast of the source body has a maximum value of –0.038 g/cm^3 (Fig. 5A) and the body itself is no thicker than 52 km, assuming that it touches the surface (Fig. 6). If the source is confined below 2.7 km depth, the density contrast cannot be everywhere greater than –0.043 g/cm^3, while the body has a thickness less than or equal to 50 km (Fig. 7). When the body is assumed to be below 8 km, the greatest density contrast is –0.092 g/cm^3, with a maximum allowable thickness of 18 km (Fig. 8). The ideal body inversions also show that the depth to the body top cannot exceed 15 km (Fig. 5). Thus, the ideal body top is required to be within the upper to middle crust and cannot be deeper. This result precludes exclusively the deep origin of the anomaly, proposed by some authors (e.g., Fajklewicz, 1964), because any density model for the PGL source body entirely located at the lower crustal level is not possible.

Previous interpretations question the possibility that the anomaly may be caused by thickening of the sedimentary cover only. One of the arguments for this conclusion is that the long-wavelength gravity anomaly related to the PGL is apparent on the residual maps after removal of the gravity effect of either the Zechstein–Cenozoic cover (Narkiewicz and Petecki, 2017: fig. 7) or the Permian-Cenozoic cover (Grobelny and Królikowski, 1988) from the Bouguer gravity data. The other arguments are the flat, layer-cake platform geometry of the Lower Paleozoic sedimentary rocks and the smooth morphology of the Precambrian crystalline basement dipping southwards along profile A–A' from 2.7 km at the Olsztyn IG 2 borehole (Fig. 3) to about 8 km at the TTZ (Fig. 2). These preclude the Lower Paleozoic structures, like a basin or a graben, filled with low-density sedimentary rocks.

The density of rocks is of essential significance for gravity data interpretation. In this study the densities of rocks of the pre-Permian sedimentary cover across the PGL region and its surrounding were analysed based on published (Królikowski et al., 1988; Dąbrowski, 1976; Grabowska et al., 1998; Modliński, 2007; Leszczyński, 2011; Podhalańska, 2012) and unpublished data collected in the Polish Geological Archive. These data indicate that the Silurian rocks have densities typically greater than 2.65 g/cm^3 (Table 1).Thus, the Lower Paleozoic rocks are not the source of the PGL anomaly. Indeed, the greatest negative density contrast expected for, e.g., 4 km thick ideal body representing the Lower Paleozoic strata is –0.3 g/cm^3 (Fig. 7), which would be an unlikely geological situation, given our present knowledge of the East European Platform sedimentary cover.

Table 1

Average density of Silurian rocks

Borehole	Depth [m]	Density [g/cm^3]
Bytów IG 1	1481–2569.7	2.58
Dretyń 1	1488–2001	2.68
Grudziądz IG 1	3029–3070.5	2.66
Kościerzyna IG 1	2097.5–4490	2.65
Malbork IG 1	2004.5–3187.5	2.64
Olsztyn IG 2	2155–2376.5	2.61
Prabuty IG 1	2487–3355	2.67
Słupsk IG 1	1150–4 490	2.68
Trzebielino 1	1377.5–2015	2.63

The Bouguer PGL anomaly can be accounted for in part by density contrasts in the post-Permian sedimentary crust (e.g., Młynarski et al., 1982; Grobelny and Królikowski, 1988; Grabowska et al., 1998), and in part by the low-density zones in the deeper zone of the crust, including the Lower Paleozoic strata and crystalline crust. Since the Lower Paleozoic rocks are not the important source of the PGL anomaly due to their high densities, the other sources must exist in the deeper part of the crust. It follows from the above considerations that the anomalous body must also be within the crystalline basement.

From the aforementioned trade-off curves, the maximum depth to the top or the minimum thickness of the source can be found for any assumed density contrast. However, there is no direct evidence for the density contrast associated with the PGL anomaly. Information on the distribution of Precambrian rock types in the PGL anomaly area is limited because of the relatively few boreholes that have penetrated into the basement and because of the complexity of the Precambrian geology in the area (Table 2; Krzemińska et al., 2017).

The deep boreholes that penetrated the crystalline basement are located in the marginal part or outside the anomaly. Six boreholes encountered 17–58 m of basement rocks such as granite,

Table 2

Crystalline basement rocks

Borehole	Rock type	Density [g/cm^3]	Thickness [m]	Chronostratigraphy
Kościerzyna IG 1	charnockitoid (AMCG)	2.71	58 m	Mezoproterozoic
Malbork IG 1	monzonite (AMCG)	–	17.3 m	Mezoproterozoic
Słupsk IG 1	granitoid	–	42 m	Paleoproterozoic
Prabuty IG 1	granite	2.68	35.4 m	Paleoproterozoic
Olsztyn IG 2	metamorphosed granite	2.79	53.8 m	Paleoproterozoic
Nidzica IG 1	granitoid	2.66	30 m	Paleoproterozoic

granitoid or AMCG (anorthosite–mangerite–charnockite–granite) suite rock with average densities in the range of 2.66–2.79 g/cm^3 (Table 2). One of them, located adjacent to the PGL and close to the A–A' profile, the Olsztyn IG 2 borehole (Fig. 3) sampled a metamorphosed granite (gneiss) with an average density of 2.79 g/cm^3.

Therefore, a minimum negative density contrast related to the PGL can be assumed for a low-density felsic body, e.g. granite, flanked by a denser metamorphic rock, such as gneiss, encountered in the Olsztyn IG 2 borehole. It may be speculated that the –0.2 g/cm^3 is a good approximation of this density contrast. Taking this value into consideration, the absolute value of density solutions for the source of the PGL is located within the shaded zones marked in Figures 5–8, in accordance with the assumptions used in the inversion process. Accordingly, the top of source body can be no deeper than 11.5 km (Fig. 5), and the body can be no thinner than 6 km, assuming it touches the surface (Fig. 6), or no thinner than 7 km, when the source is confined below 8 km depth (Fig. 8). The shallower depths and greater thicknesses are indicated by adopting greater negative density contrasts.

It is impossible to check precisely the validity of the previous models (Grabowska and Raczyńska, 1991; Grabowska et al., 1992; Królikowski and Petecki, 1997, 2002; Petecki, 2002, 2008; Mazur et al., 2015, 2016a, b) by plotting their minimum density contrast in Figures 5–8, because these models present the results of gravity forward modelling, focusing on the complex structure of the crust and uppermost mantle across the TTZ. Nevertheless, the gravity models explaining the PGL anomaly by the lower crustal thickening only (Królikowski and Petecki, 2002; Petecki, 2002; Mazur et al., 2015, 2016a, b) are not confirmed by the present results. Furthermore, the depth to the top of source body (less than or equal to 10 km), as predicted by Młynarski et al. (1982), is located within the acceptable range of solutions (shaded zone in Fig. 5), consistent with the geological and geophysical constraints imposed on the data in the ideal body inversion procedure. Nevertheless, the minimum thickness of the body (2.7 km), estimated by Młynarski et al. (1982), is inconsistent with these constraints (Figs. 6–8).

A geological explanation of the ideal body related to the PGL is beyond the scope of this paper. Moreover, we have only limited knowledge of the crystalline basement geology in the studied area (as summarized by Krzemińska et al., 2017) due to the lack of an adequate borehole control. Therefore, a convincing interpretation of the possible structure (-s) responsible for the PGL is hardly possible. It can be merely hypothesized that the main source of the negative gravity anomaly is related to a predominance of felsic rocks in the Dobrzyń Domain of Paleoproterozoic age (Petecki and Rosowiecka, 2017; Krzemińska et al., 2017). Granites, found below the basement top in a few deep boreholes in the NE part of the PGL, are consistent with such a general and tentative supposition.

However, as the results of ideal body inversion (Figs. 5–8) allow for ideal body occupying the whole crystalline crust, the PGL anomaly may represent a tectonic feature of the EEC boundary zone in this region, e.g. the inclination of crystalline basement strata.

CONCLUSIONS

The absolute value of gravity anomaly along the profile crossing the PGL was inverted using Parker's ideal body theory to find some parameters of the source body with the smallest maximum density contrast that satisfies the data and their associated errors. In the ideal body inversion procedure, it was not possible to define the geometry of the causative body, but this analysis provided limits on the density contrast, depth, and minimum thickness of the causative body.

The ideal body inversion clearly shows that the top of the source of the PGL is buried no deeper than 15 km (Fig. 5A). Assuming the geologically reasonable minimum density contrast of –0.2 g/cm^3, the maximum depth of the source top is 11.5 km (Fig. 5). Even shallower depths are indicated by assuming greater negative density contrasts. In addition, the present results demonstrate that the amplitude of the PGL is too high to be connected only with a regional thickening of Paleozoic–Mesozoic sediments.

The PGL residual gravity can be explained partly by a set of sources located in the upper sedimentary crust and partly by a low-density zone at the crystalline crustal level. This model is consistent with information from boreholes, density measurements, and other geophysical interpretations (Młynarski et al., 1982; Grobelny and Królikowski, 1988; Grabowska et al., 1998).

The ideal body optimization results indicate the crustal origin of the PGL, i.e. presence of a low-density body located in the crust. The present study also demonstrates that the PGL anomaly cannot be explained by a narrow crustal root (Mazur et al., 2015) or a wide zone of crustal thickening (Fajklewicz, 1964; Królikowski and Petecki, 2002; Petecki, 2002) alone, because any geological model of the PGL involving only a lower crustal level is inacceptable. In view of the present results, the negative residual gravity anomaly may be related to a predominance of felsic rocks in the Paleoproterozoic granitic Dobrzyń Domain shown on the geological map of crystalline basement in the Polish part of the East European Platform (Ryka, 1982; Krzemińska et al., 2017). This conclusion does not rule out the presence of a low-density zone in the whole crystalline crust, which may represent a tectonic feature of the EEC boundary zone in this region.

The current results neither support nor exclude the presence of a subordinate gravity contribution from additional sources, e.g. from a hypothetical crustal keel. Future investigations of possible complexities of the actual density distribution related to the PGL will require application of other geophysical methods, e.g. traditional gravity modelling combined with the ideal body analysis.

Acknowledgements. The author is grateful to M. Bielik and L. Krysiński for their constructive comments and improvements to the text. Prof. M. Narkiewicz is warmly acknowledged for valuable discussions and useful suggestions on the original manuscript.

REFERENCES

Ander, E., Huestis, S.P., 1987. Gravity ideal bodies. Geophysics, **52**: 1265–1278.

Blakely, R.J., 1995. Potential Theory in Gravity and Magnetic Applications. Cambridge University Press, Cambridge.

Dąbrowski, A., 1976. Mean densities of Pre-Devonian sedimentary rocks in Poland and their depth dependence. Pageoph, **114**: 251–262.

Fajklewicz, Z., 1964. Głębokość zalegania nieciągłości Mohorovičica w Polsce (in Polish). Technika Poszukiwań, **10**: 6–11.

Grabowska, T., Raczyńska, M., 1991. Structure of the Earth crust in the Polish Lowland in the light of gravimetric modelling. Publications of the Institute of Geophysics, Polish Academy of Science, **A-19**: 85–110.

Grabowska, T., Raczyńska, M., Dolnicki, J., 1992. Interpretation of gravity anomalies along the Eu-3 Geotransect in Poland. Acta Geophysica Polonica, **40**: 159–173.

Grabowska, T., Bojdys, G., Dolnicki, J., 1998. Three-dimensional density model of the Earth's crust and the upper mantle for the area of Poland. Journal of Geodynamics, **25**: 5–24.

Grobelny, A., Królikowski, C., 1988. Gravimetric anomalies caused by sub-Permian sediments in northwestern Poland (in Polish with English summary). Kwartalnik Geologiczny, **32** (3/4): 611–634.

Guterch, A., Grad, M., 2006. Lithospheric structure of the TESZ in Poland based on modern seismic experiments. Geological Quarterly, **50** (1): 23–32.

Huestis, S.P., 1986. Uniform norm minimization in three dimensions. Geophysics, **51**: 1141–1145.

Huestis, S.P., Ander, E., 1983. IDB2 – a Fortran program for computing extremal bounds in gravity data interpretation. Geophysics, **47**: 999–1010.

Królikowski, C., Petecki, Z., 1995. Atlas grawimetryczny Polski (in Polish). Państwowy Instytut Geologiczny, Warszawa.

Królikowski, C., Petecki, Z., 1997. Crustal structure at the Trans-European Suture Zone in northwest Poland based on gravity data. Geological Magazine, **134**: 661–667.

Królikowski, C., Petecki, Z., 2002. Lithospheric structure across the Trans-European Suture Zone in NW Poland based on gravity data interpretation. Geological Quarterly, **46** (3): 235–245.

Królikowski, C., Petecki, Z., Żółtowski, Z., 1998. Main structural units in the Polish part of the East-European Platform in the light of gravimetric data (in Polish with English summary). Biuletyn Państwowego Instytutu Geologicznego, **386**: 5–58.

Królikowski, C., Bronowska, E., Dąbrowski, A., Bujnowski, W., Jasiński, Z., Grobelny, A., Twarogowski, J., 1988. The distribution of the density of Cainozoic and Permian-Mesozoic rocks in north-western Poland (in Polish with English summary). Prace Instytutu Geologicznego, **124**:1–114.

Krzemińska, E., Krzemiński, L., Petecki, Z., Wiszniewska, J., Salwa, S., Żaba, J., Gaidzik, K., Williams, I.S., Rosowiecka, O., Taran, L., Johansson, Å., Pécskay, Z., Demaiffe, D., Grabowski, J., Zieliński, G., 2017. Geological Map of Crystalline Basement in the Polish part of the East European Platform 1:1 000 000. Państwowy Instytut Geologiczny, Warszawa.

Leszczyński, K., 2011. Grudziądz IG 1 (in Polish with English summary). Profile Głębokich Otworów Wiertniczych Państwowego Instytutu Geologicznego, **129**.

Mazur, S., Mikołajczak, M., Krzywiec, P., Malinowski, M., Buffenmyer, V., Lewandowski, M., 2015. Is the Teisseyre-Tornquist Zone an ancient plate boundary of Baltica? Tectonics, **34**: 465–2477.

Mazur, S., Mikołajczak, M., Krzywiec, P., Malinowski, M., Buffenmyer, V., Lewandowski, M., 2016a. Reply to Comment by M. Narkiewicz and Z. Petecki on "Is the Teisseyre-Tornquist Zone an ancient plate boundary of Baltica?" Tectonics, **35**: 1600–1607.

Mazur, S., Mikołajczak, M., Krzywiec, P., Malinowski, M., Lewandowski, M., Buffenmyer, V., 2016b. Pomeranian Caledonides, NW Poland – a collisional suture or thin-skinned fold-and-thrust belt? Tectonophysics, **692**: 29–43.

Młynarski, S., Bachan, W., Dąbrowska, B., Jankowski, H., Kaniewska, E., Karaczun, K., Kozera, A., Marek, S., Skorupa, J., Żelichowski, A.M., Żytko, K., 1982. Geophysical-geological interpretations along the profiles of Lubin-Prabuty, Przedbórz-Żebrak, Baligród-Dubienka (in Polish with English summary). Biuletyn Instytutu Geologicznego, **333**: 5–60.

Modliński, Z., 2007. Słupsk IG 1 (in Polish with English summary). Profile Głębokich Otworów Wiertniczych Państwowego Instytutu Geologicznego, **116**.

Narkiewicz, M., Petecki, Z., 2016. Comment on "Is the Teisseyre-Tornquist Zone an ancient plate boundary of Baltica?" by Mazur et al. Tectonics, **35**: 1595–1599.

Narkiewicz, M., Petecki, Z., 2017. Basement structure of the Palaeozoic Platform in Poland. Geological Quarterly, **61** (2): 502–520.

Narkiewicz, M., Maksym, A., Malinowski, M., Grad, M., Guterch, A., Petecki, Z., Probulski, J., Janik, T., Majdański, M., Środa, P., Czuba, W., Gaczyński, E., Jankowski, L., 2015. Transcurrent nature of the Teisseyre-Tornquist Zone in Central Europe: results of the POLCRUST-01 deep reflection seismic profile. International Journal of Earth Sciences, **104**: 775–796.

Parker, R.L., 1974. Best bounds on density and depth from gravity data. Geophysics, **39**: 644–649.

Parker, R.L., 1975. The theory of ideal bodies for gravity interpretation. Geophysical Journal of the Royal Astronomical Society, **42**: 315–334.

Petecki, Z., 2002. Gravity and magnetic modeling along LT-7 profile (in Polish with English summary). Przegląd Geologiczny, **50**: 630–633.

Petecki, Z., 2008. Magnetic basement in the Pomeranian segment of the Trans-European Suture Zone (NW Po land) (in Polish with English summary). Prace Państwowego Instytutu Geologicznego, **191**: 5–72.

Petecki, Z., Rosowiecka, O., 2017. A new magnetic anomaly map of Poland and its contribution to the recognition of crystalline basement rocks. Geological Quarterly, **61** (4): 934–945.

Podhalańska, T., 2012. Malbork IG 1 (in Polish with English summary). Profile Głębokich Otworów Wiertniczych Państwowego Instytutu Geologicznego, **136**.

Ryka, W., 1982. Precambrian evolution of the Polish part of the East-European Platform (in Polish with English summary). Kwartalnik Geologiczny, **26** (2): 257–272.